Engineering Structures 297 (2023) 116957

Contents lists available at ScienceDirect

Engineering Structures

journal homepage: www.elsevier.com/locate/engstruct

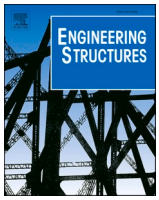

Strain-Based elevation monitoring during construction of the Salesforce Tower

Jordan K. Baldwin [a,*], Philip M. Gullett [b], Isaac L. Howard [c]

[a] Principal Engineer / Surveyor, President & CEO, Ridgeline Engineering, 2769 Boeing Way, Stockton, CA 95206, United States
[b] Associate Professor, Richard A. Rula School of Civil & Environmental Engineering, Mississippi State University, 250 Hardy Road, Mississippi State, MS 39762, United States
[c] Professor and Director, Richard A. Rula School of Civil & Environmental Engineering, Mississippi State University, 250 Hardy Road, Mississippi State, MS 39762, United States

A B S T R A C T

Anticipated complexities associated with monitoring elevation changes during construction of the 326 m tall Salesforce Tower in San Francisco prompted the implementation of a strain-based system. This system utilizes strain gages embedded into the tower's reinforced concrete walls and the resulting measurements are inputs into one of three shortening estimation models of varying complexity and applicability. This methodology was successfully utilized to monitor time dependent shortening due to axial, shrinkage, and creep strains in the tower. Strain-gage based systems assist with slender tower construction in urban areas because the tower's slenderness coupled with adjacent obstacles stretch the limits of traditional or alternative instrument capabilities and they provide redundancy of measurement to ensure accuracy. This paper is a case study of how a strain-based elevation monitoring system helped this project to be successful. The most relevant findings are: 1) the shortening estimation models were in agreement with conventional survey measurements (±4.6 mm) within their recommended tower height and temperature range capabilities; 2) implementation of this system resulted in a net monitoring cost reduction on the order of 15 %, 400 less labor hours, and reduced potential for project delays; and 3) improvements are needed for supplying power to the sensors as there were interruptions, cut cables, and lack of sources that led to a 44 % sensor success rate. Given the need for structural health monitoring, the successful outcomes documented in this paper, and the potential for continued improvement by way of, for example, wireless and battery free sensing technologies, the work documented herein is believed to be an incremental advancement to the state-of-the-art of tall buildings.

1. Introduction

Tall buildings serve an obvious functional purpose as population density continues to rise in cities, but are also a symbol of economic growth, status, and power (Domosh [1]). According to the Council on Tall Buildings and Urban Habitat [CTBUH] Skyscraper Center [2], nearly half of the 100 tallest buildings standing were constructed within the past five years and the number of newly constructed buildings 300 m or taller, known as 'supertall' buildings, has increased from a five-year rolling average of one per year in 2003 to twenty-one in 2022. Additionally, the construction of buildings 600 m or taller, known as 'megatall' buildings, is also increasing with three fully constructed buildings to date, two currently under construction, six scheduled for construction, and 52 more in conceptual design.

During construction of tall buildings, elevations are benchmarked at intermittent levels throughout the height of the tower. As construction proceeds upward, benchmarks are used as reference to ensure each new story is correctly built to the designed elevation. The accuracy of benchmark elevations is affected throughout construction as a building shortens due to the development of axial strain, which can lead to inconsistencies and problems such as uneven floor levels or structural members and architectural components that do not fit as intended (Fintel et al. [3]). Conventional methods, such as steel tape, total station, and GNSS (Global Navigation Satellite System) have traditionally been used to monitor benchmark elevations (Ghilani [4]). However, the practical application of these methods is limited by tower height. For instance, the labor necessary to repeatedly traverse up and down a tall tower with steel tape or total station instruments can become extensive and line of sight and visibility complications become more pronounced with height. Conversely, due to reduced obstructions, GNSS receivers generally perform better at greater heights.

Strain-based elevation monitoring is not necessarily limited by height and was incorporated to compliment and be used in conjunction with these current methods during construction of the Salesforce Tower in San Francisco, CA. While some studies have explored the use of strain gauges to monitor axial strain development within individual members,

* Corresponding author.
E-mail addresses: jordan@rle.us (J.K. Baldwin), pmgullett@cee.msstate.edu (P.M. Gullett), ilhoward@cee.msstate.edu (I.L. Howard).

https://doi.org/10.1016/j.engstruct.2023.116957
Received 8 April 2023; Received in revised form 22 August 2023; Accepted 22 September 2023
Available online 6 October 2023

the primary contribution of this case study is that it presents a practical approach to estimate elevation changes throughout a multi-story reinforced concrete core wall tower during construction.

2. Project configuration

The tip of the Salesforce Tower reaches 1,070 feet (326 m) above grade. The first 961 feet (293 m) contains 63 stories below the roof while the remainder consists of an open-air screen wall. The structure also extends below grade 55 feet (17 m), housing three parking garage levels. The inner core consists of a square and biaxially centered reinforced concrete core wall with an 88.67 feet (27.0 m) interior clear width. The core walls throughout the tower range from 48 in. (1.2 m) thick at the base to 24 in. (0.6 m) thick at the top and are comprised of the same high-strength concrete with a 28-day compressive strength of 11.9 ksi (81.9 MPa), slump of 9 in (230 mm), and 0.75 in (19 mm) maximum sized coarse aggregates. The core is split in half with a dividing wall spanning in the east to west direction. Fig. 1A illustrates the tower plan layout which includes the central core wall and perimeter steel columns supporting reinforced concrete decking and a glass curtain wall. Fig. 1B and 1C are of core wall construction while Fig. 1D depicts the finished glass exterior. Project specifications required that benchmark elevations be established and subsequent changes in elevations be periodically monitored approximately every eight stories until the 60th level was completed. Total station and strain measurements were selected as the primary methods for monitoring these elevation changes.

Strains were measured using steel encased vibrating wire strain gauges, manufactured by Soil Instruments Ltd. The gauges were embedded within the concrete walls and detect strain changes by measuring frequency changes when the gauge wire is tightened or relaxed. The gauges have a range of 3,000 με (microstrain) which is about six times the expected maximum, based on other tower modeling and monitoring results (Peronto, et al. [5]; Abdelrazaq [6]). Studies have observed that gauges must be long enough to closely capture the general response amid localized stress concentrations, indicating measurement errors of less than ±5 % when gauge lengths are at least five times the maximum aggregate dimension (Geymayer [7]; Bakoss et al. [8]). The gauges were 157 mm long, exceeding eight times the maximum aggregate dimension, and contained 19 mm diameter flanges at both ends. The presence of flanges promotes interlocking with the surrounding concrete, reducing shear stresses and the potential for slippage along the gauge length (Hameed et al. [9]). One gauge was embedded within each of the four walls of an instrumented story (Fig. 1A) to provide some measurement redundancy. The gauges were placed in the center of the wall section, oriented vertically, and tied to the longitudinal wall reinforcement (Fig. 1E). Cables were channeled from the four gauges to a Geokon LC-2x4 Datalogger (4 channel), where changes in the vibrating wire frequencies were translated to changes in strain and passed through a Sensemetrics X-Series Thread, which wirelessly transmitted the data in real-time (Fig. 1F). To better understand how these strain gauge measurements can be interpreted to estimate shortening, predicted axial strain development throughout a multi-level tower was examined.

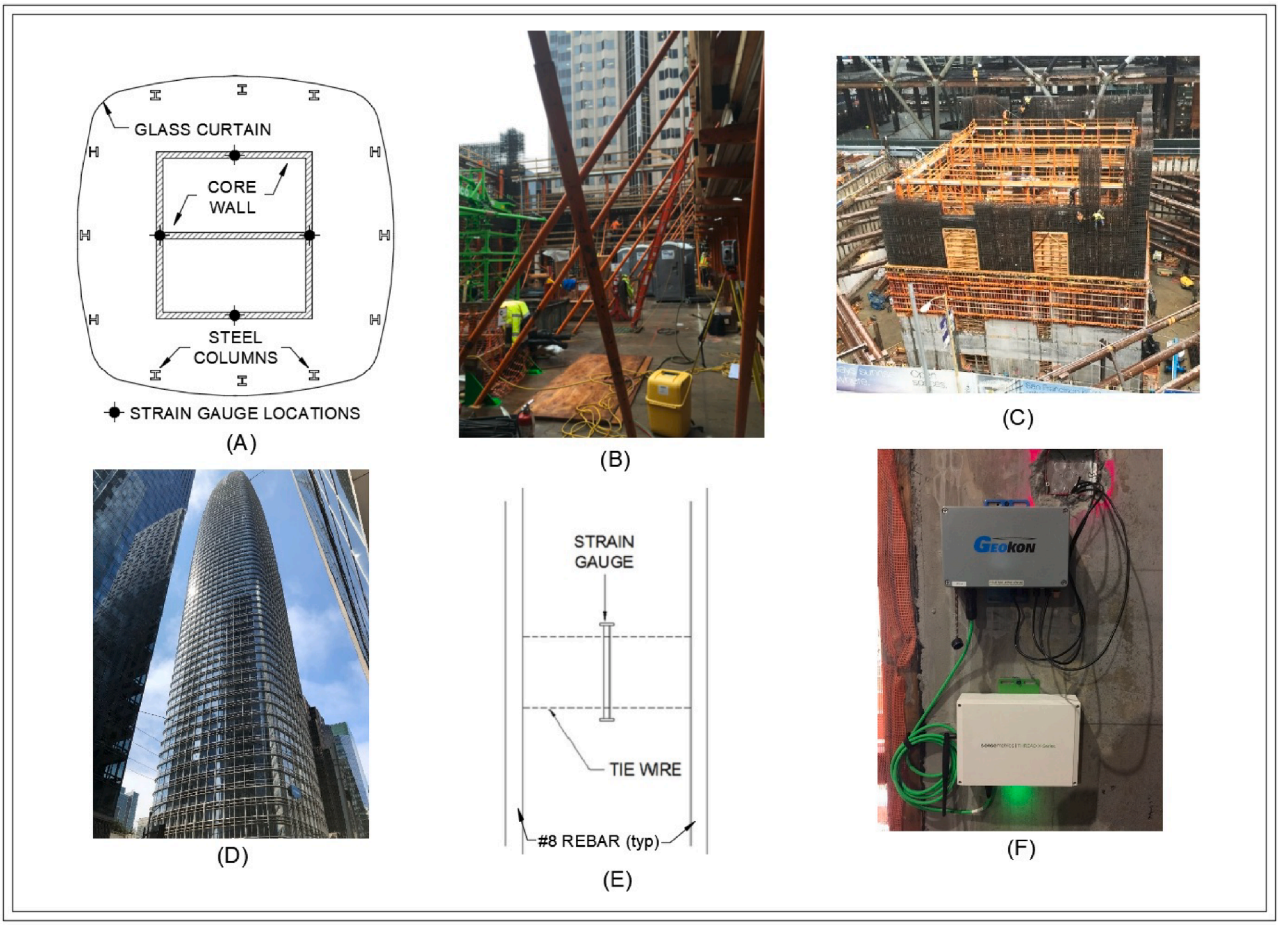

Fig. 1. (A) Tower plan layout, (B) Inside core wall construction, (C) outside core wall construction, (D) Glass curtain wall nearing completion, (E) Illustration of gauge tied between reinforcement bars, (F) Geokon datalogger and Sensemetrics Thread.

3. Approximate tower strain development

This section reviews fundamental concepts of concrete strain development and defines a simplified approach to approximating a tower strain profile. The primary fundamental concept considered is the fact that concrete members shorten over time due to the development of axial strains, specifically the sum of compressive elastic ε_e, creep ε_c, and shrinkage ε_{sh} strains (Bazant [10]). Both creep and shrinkage strains are time-dependent and develop in a logarithmic fashion. Because stories of a core wall tower are formed and poured at different points in time, each develops strains uniquely relative to each other. Compressive elastic strains develop as the weight of a newly constructed story imposes stress, σ, upon a previously constructed story, and depend on the concrete elastic modulus, E_c, at the time the stress is applied, t'. Creep strains are approximately related to stress when in service ranges, indicated by a creep coefficient, φ, and defined as the ratio of the creep deformation to the initial elastic deformation. Because multiple stories, n, impose instances of stress, strains produced in each instance can be summed together based on the principle of superposition to approximate totals. Shrinkage strains develop as the concrete matures and are a function of the time that curing concludes and drying commences, t_0. Based on these fundamental concepts, the method to approximate strain, ε, developed within a given story at a point in time, t, may be predicted as:

$$\varepsilon(t,t') = \sum_{i=1}^{n}\left(\frac{1+\varphi(t,t_i')}{E_c(t_i')}\right)\sigma(t_i') + \varepsilon_{sh}(t,t_0) \quad [1]$$

The first term of the equation combines elastic and creep strains and is considered the stress-dependent strain, ε_σ.

After a story is formed and poured but before stress is imposed and drying commences, Eq. [1] predicts axial strain to be zero even though it will vary linearly along the height of the wall due to self-weight. This initial condition is absent from the prediction equation which assumes a uniform strain profile, similar to the incremental change of the strain profile which is approximately constant. This approximation is considered acceptable for purposes of monitoring because incremental changes in strain, instead of total strain, are measured by gauges and used to estimate incremental height changes.

Fig. 2 illustrates an example of a predicted strain profile for the bottom eight stories of a tower between an initial reference time, t_r, and current time, t, where compressive strains are considered positive. Because the concrete is younger at the reference time, differences throughout the profile are more pronounced due to the rapid development of logarithmic-style creep and shrinkage strains. At later ages, these differences reduce as the rate of strain development lessens. The difference between the two strain profiles gives the incremental change in strain occurring between the two points in time, $\Delta\varepsilon$, and the solid vertical line illustrates the average change, $\overline{\Delta\varepsilon}$. Shortening within the segment, Δh, can be approximated by multiplying the average change in strain by the height, h, and the elevation of level eight at time t can be approximated by subtracting segment shortening from the elevation at time t_r. To measure and compute the actual average change in strain, gauges would need to be installed within each story of the tower. During construction of the Salesforce Tower, gauges were installed approximately every eight stories, producing an average measured change in strain, $\overline{\Delta\varepsilon}_g$, that is different than the actual average change, as illustrated by the gap between the solid and dashed vertical lines in Fig. 2. This difference required the average change in strain to be estimated.

4. Tower shortening estimation methods

Three methods of varying complexity were developed to estimate the average change in strain, alongside subsequent shortening and elevation changes, within a tower using strain measurements acquired at intermittent levels. Table 1 indicates the change in strain estimation parameters used in each method. Because the change in strain profile of a tower segment resembles a linear trend, each method linearly interpolates gauge measured changes in strain to compute the average gauge measured change in strain, as illustrated by the dashed line in Fig. 2. In addition, Method B incorporates a coefficient of thermal expansion (CTE) adjustment to the strain gauge measurements, while Method C attempts to approximate the non-linear change in strain (the

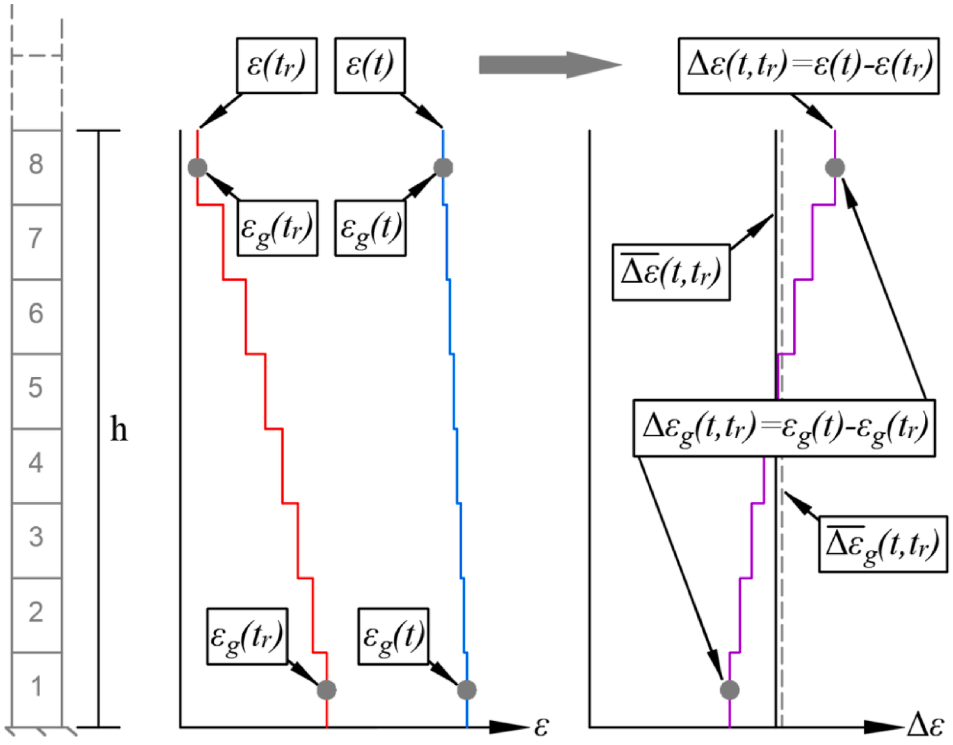

Fig. 2. Tower Strain Profile Example.

Table 1
Summary of Parameters Associated with Tower Shortening Estimation Methods.

Parameter	A	B	C
Measured strain change ($\Delta\varepsilon$)	✔	✔	✔
Height between instrumented levels (h)	✔	✔	✔
Measured temperature change (ΔT)		✔	✔
Material CTE difference ($\Delta\alpha$)		✔	✔
Reinforcement ratio (longitudinal)			✔
Span between instrumented levels (m)			✔
Concrete age when measurements begin (t_r)			✔
Concrete age when measurements end (t)			✔
Prediction model results (ACI, B3, CEB, GL, B4)			✔

difference between the solid and dashed vertical lines illustrated in Fig. 2) using results from concrete strain prediction models.

Table 2 outlines parameters associated with a variety of concrete strain prediction modeling criteria developed by Bazant & Baweja [11] (B3), Gardner & Lockman [12] (GL), American Concrete Institute Committee 209 [13] (ACI), Comité Euro-International du Béton [14] (CEB), and Bazant et al. [15] (B4). Though these modeling criteria would typically be incorporated into complex computer modeling when analyzing strain development throughout a tower, here they are used to supplement strain gauge measurements using a simplified approach, based on Equation [1]. Timely implementation using routine software and computing power motivated the simplified use of these models.

4.1. Tower shortening estimation Method components

For purposes of estimating shortening, the tower was divided into segments. Segments span between instrumented levels so that each segment contains strain measurements at either end. The average change in strain for segment q containing m stories can be estimated as:

$$\overline{\Delta\varepsilon}_q(t,t_\tau) = \frac{1}{2}[\Delta\varepsilon_{1,q}(t,t_r) + \Delta\varepsilon_{m,q}(t,t_r) + \chi_q(t_r,t,m)] \quad [2]$$

The gauge measured changes in strain values at levels 1 and m are used for Method A, but are adjusted for differences in CTE between the member and gauge in Methods B and C. The second term of the equation equals zero for Methods A and B, but accounts for the approximated non-linear change in strain in Method C. Shortening within segment q is then estimated by multiplying the average measured change in strain by the segment height, h_q:

$$\Delta h_q(t,t_r) = \overline{\Delta\varepsilon}_q(t,t_r)h_q \quad [3]$$

Benchmark levels higher in the tower contain multiple segments below their level. Total estimated cumulative shortening encompassing p segments is found by summing estimated shortening within each individual segment:

$$\Delta H_p(t,t_r) = \sum_{q=1}^{p}\Delta h_q(t,t_r)\Delta h_q(t,t_r) \quad [4]$$

The adjusted benchmark elevation at the top of segment p is computed as:

$$EL_p(t) = \mathrm{EL_p}(t_r) - \Delta H_p(t,t_r) \quad [5]$$

Table 2
Summary of Parameters Associated with Concrete Strain Prediction Models.

Parameter	ACI	B3	CEB	GL	B4
Curing duration	✔	✔	✔	✔	✔
Curing condition	✔	✔			
Relative humidity	✔	✔	✔	✔	✔
Volume to surface ratio	✔	✔	✔	✔	✔
Cement type	✔	✔	✔	✔	✔
Concrete slump	✔				
Fine aggregate percentage	✔				
Air percentage	✔				
Cement content	✔	✔			✔
Water content		✔			✔
Aggregate content		✔			✔
Type of aggregate			✔		✔
Concrete 28-day strength		✔	✔	✔	✔
Concrete age when loaded	✔	✔	✔	✔	✔
Member shape		✔			✔
Admixtures					✔

4.2. CTE adjustment

Due to differing CTE values, a strain gauge made of steel is inclined to expand and contract differently than the surrounding concrete. The restraint causes the gauge to be stressed as though it is being pushed or pulled causing "apparent" strains to be registered by the gauge even though they do not actually exist within the concrete. These effects are largely corrected by adjusting the measured change in strain values by the product of the difference in CTE between the gauge and surrounding concrete, $\Delta\alpha$, and the change in measured temperature, ΔT (Batten et al. [16]). The coefficient of thermal expansion of the tower concrete mix was specified as 13.2 με/°C compared to 12.2 με/°C specified for the gauge (Soil Instruments [17]), indicating a difference of approximately 1.0 με/°C. The strain gauges contained temperature sensors which allowed this adjustment to be made. In general, the relative impact of CTE adjustments decrease as wall strains increase, indicating adjustments may be more critical when strains are smaller and temperature swings are larger.

4.3. Non-linearity prediction

To estimate and adjust for the non-linear behavior that the first term of Equation [2] fails to capture, axial compressive, creep, and shrinkage strain development predictions based on anticipated parameter values were prepared prior to construction. Although the use of as-built conditions may improve modeling accuracy, benchmark elevations needed to be frequently updated and utilized throughout the duration of construction, requiring models to be prepared beforehand. Simplified models based on Eq. [1] were developed for a typical story using ACI, B3, CEB, GL, and B4 prediction modeling criteria. Because each model exhibits varying dependencies and sensitivities to parameters under consideration, a range of predictions were produced and overlaid (Fig. 3). As an example, the process used to develop the ACI prediction model results are demonstrated in the following section.

4.3.1. ACI predictions

ACI 209 [13] predicts the creep and shrinkage components in Eq. [1] by first estimating ultimate creep, φ_u, and ultimate shrinkage, ε_{shu}, terms, which represent the maximums a member is expected to experience after an extended period of time. In the absence of specific shrinkage and creep data for local aggregates and conditions, ACI suggests standard values for standard conditions of 2.35 and 780 με for creep and shrinkage, respectively. Some standard conditions include an ambient relative humidity of 40 %, a volume-to-surface ratio of 1.5 in (38 mm), a fine aggregate percentage of 50 %, and a slump of 2.7 in (70 mm). A series of correction factors are used to modify standard values for deviating conditions. Table 3 details each of the correction factors with their corresponding ACI equation number and their association with parameters specific to the Salesforce Tower concrete, average expected relative humidity, and average member volume to surface ratio. ACI incorporates the ultimate values with a time-based logarithmic-style development curve to estimate values at any point in time, t. These values were used in conjunction with an anticipated incremental stress of 16 psi (110 kpa) imposed every 5 days due to new story construction and a specified 28-day concrete compressive strength of 11.9 ksi (81.9 MPa), to develop the ACI model graphically presented in Fig. 3 and partially detailed numerically in Table 4.

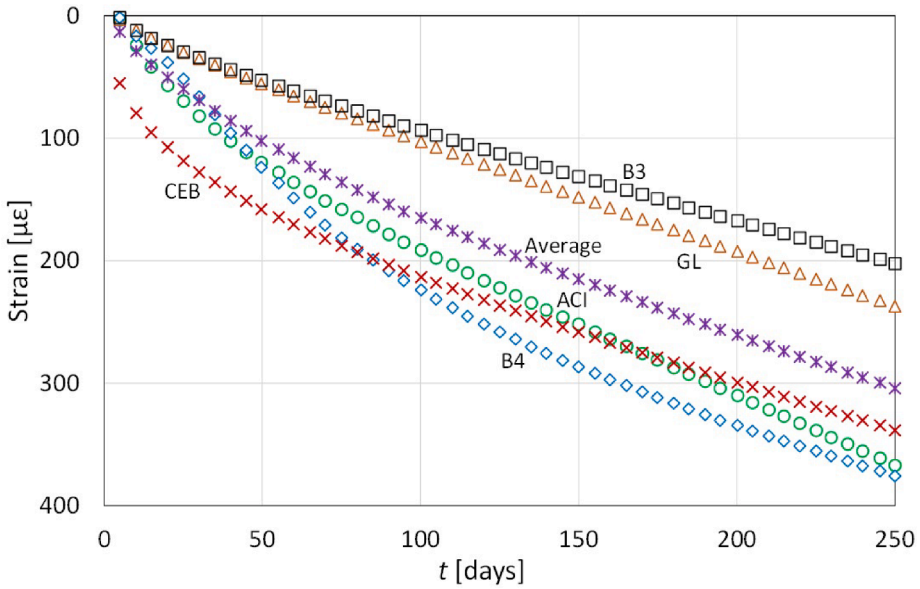

Fig. 3. Simplified Strain Development Predictions.

Table 3
ACI Ultimate Shrinkage Strain and Creep Coefficient Factors.

Input Parameter		Shrinkage Factors			Creep Factors		
Curing time, t_o [days]	5	$\gamma_{sh,to}$ =	1.04	(A-6)	$\gamma_{c,to}$ =	1.00	(A-22)
Humidity, h	0.7	$\gamma_{sh,h}$ =	0.69	(A-7)	$\gamma_{c,h}$ =	0.80	(A-24)
Vol. to surf. ratio, vs [mm]	380	$\gamma_{sh,vs}$ =	0.20	(A-8)	$\gamma_{c,vs}$ =	0.67	(A-25)
Slump, s [mm]	230	$\gamma_{sh,s}$ =	1.26	(A-11)	$\gamma_{c,s}$ =	1.42	(A-28)
Fine aggregate, g [%]	50	$\gamma_{sh,g}$ =	1.00	(A-12)	$\gamma_{c,g}$ =	1.00	(A-29)
Cement content, c [kg/m3]	470	$\gamma_{sh,c}$ =	1.03	(A-13)			
Air content, a [%]	2.48	$\gamma_{sh,a}$ =	1.00	(A-14)	$\gamma_{c,a}$ =	1.00	(A-30)
Note: (A-6) to (A-29) are ACI 209		γ_{sh} =	0.18	(A-5)	γ_c =	0.76	(A-21)
[13] equation numbers		**ε_{shu} [με] =**	**143.6**	(A-4)	**φ_u =**	**1.786**	(A-20)

Columns (3) through (6) of Table 4 lists truncated results from the stress-dependent term of Eq. [1] for i equal to 1 through 10, with the summation in Column (7). Because prediction criteria are based on a database of plain concrete materials, total predictions listed in Column (9) were adjusted to account for reinforcement effects, ε_r, in Column (10). Adjustments were made, based on an average longitudinal reinforcement ratio of 0.008 given in the structural plans of the Salesforce Tower, by equating predicted strains to compressive strains resulting from a fictitious axial force that is distributed over the concrete and steel areas (Gribniak et al. [18]). Fig. 4 illustrates the first two stress applications with values from the first two rows of Table 4.

Although these values represent the predicted axial strain development within the bottom story of a typical core wall segment, they will similarly represent the predicted axial strain development within any story assuming the same input parameters are expected (e.g. material properties, stresses, environmental conditions, and construction sequencing). Table 5 demonstrates this relationship for each story in an eight-level segment, where Level 1 is aged 50 days in Column (1), 45 days in Column (2), and the change in strain between the two periods is indicated in Column (3). The average change in predicted strain, $\overline{\Delta\varepsilon_r}$, is presented below along with a hypothetical average change in measured strain, $\overline{\Delta\varepsilon_g}$, which assumes gauges installed within Levels 1 and 8 record values equal to those predicted. Due to this assumption, the difference between the two averages is considered an approximation of nonlinearity, χ, that is uncaptured by the simplified linear interpolation between gauges.

Table 4
ACI Modeled Strain Development.

(1)	(2)	(3)	(4)	(5)	(6)	(7)	(8)	(9)	(10)
n	t [days]	$\varepsilon_\sigma(t,t_1')$ [με]	$\varepsilon_\sigma(t,t_2')$ [με]	…	$\varepsilon_\sigma(t,t_{10}')$ [με]	$\varepsilon_\sigma(t,t')$ [με]	$\varepsilon_{sh}(t,t_0)$ [με]	$\varepsilon(t,t')$ [με]	$\varepsilon_r(t,t')$ [με]
1	5	3.31				3.31	0.00	3.31	3.16
2	10	4.54	2.88			7.42	17.95	25.37	24.33
3	15	4.99	3.95	…		11.66	31.90	43.56	41.84
4	20	5.30	4.34	…		16.01	43.07	59.08	56.79
5	25	5.53	4.61	…		20.46	52.21	72.67	69.87
6	30	5.72	4.81	…		24.98	59.82	84.80	81.58
7	35	5.88	4.98	…		29.57	66.26	95.83	92.22
8	40	6.01	5.12	…		34.23	71.78	106.01	102.04
9	45	6.13	5.23	…		38.94	76.57	115.51	111.20
10	50	6.24	5.34	…	2.5	43.70	80.76	124.46	119.84

Note: (1) to (10) are column identifiers.

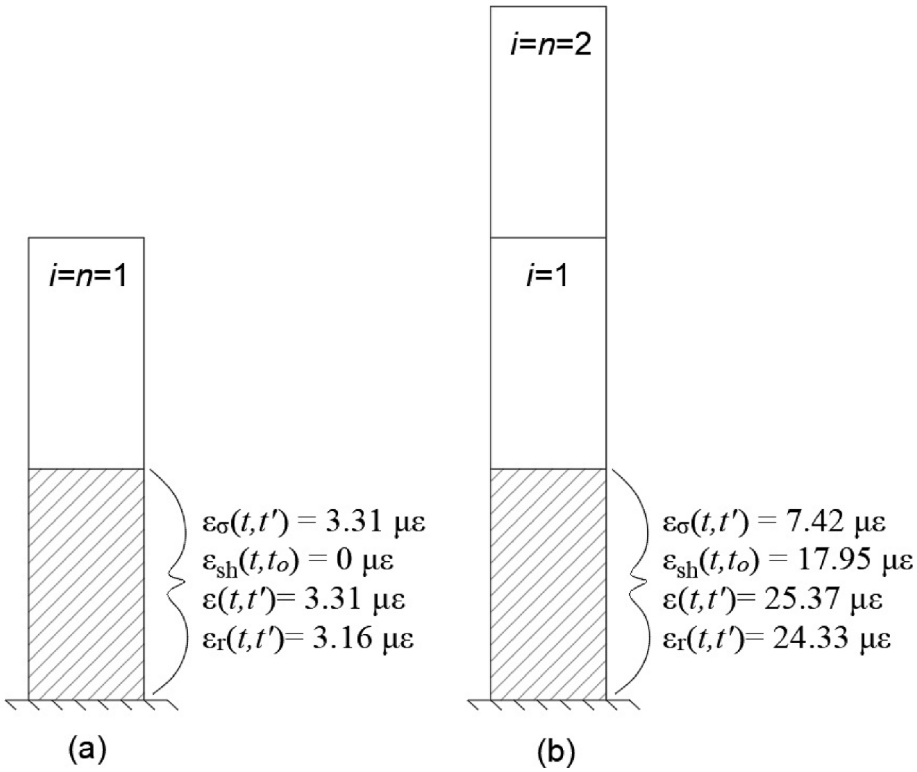

Fig. 4. Strain Development at (a) $t = 5$ and (b) $t = 10$.

Table 5
Approximate Non-linearity Prediction ($t_r = 45$; $t = 50$).

Level	(1) $\varepsilon_r(t_{50},t')$ [με]	(2) $\varepsilon_r(t_{45},t')$ [με]	(3) $\Delta\varepsilon_r(t_{50}, t_{45})$ [με]
1	119.84	111.20	8.64
2	111.20	102.04	9.16
3	102.04	92.22	9.82
4	92.22	81.58	10.64
5	81.58	69.87	11.70
6	69.87	56.79	13.09
7	56.79	41.84	14.95
8	41.84	24.33	17.51
		$\overline{\Delta\varepsilon_r}(t_{50},t_{45})=$	11.94
		$\overline{\Delta\varepsilon_g}(t_{50},t_{45})=$	13.07
		$\chi(t_{50},t_{45})=$	−1.14

4.3.2. Regression modeling of non-linearity predictions

To capture the range of variability amongst prediction model results, as exhibited in Fig. 3, non-linearity prediction results, χ, were calculated and compiled for ACI, B3, CEB, GL, and B4 for all expected combinations of t_r (between 10 and 115 days after the top story of a segment is poured, at 5 day intervals), t (between 10 days after t_r and 260 days after the top story of a segment is poured, at 5 day intervals), and m (between 5 and 8 stories, at 1 story intervals). The time parameter ranges were selected to encompass the expected project duration and the story range was selected to accommodate some variation in sensor spacing. The resulting 16,940 model data points are illustrated in Fig. 5 when plotted against each of the three independent variables. In general, greater variations in χ values can be observed at lower values of t_r and t and higher values of m. Computation of the coefficient of determination (R^2) was used to estimate best fit in each case. A linear fit proved best for t_r and m, whereas a logarithmic function slightly improved fit for the t plot. Using the method of least squares, a multivariable regression model was developed (Mendenhall & Sincich [19]) and is presented as Eq. [6] within Fig. 5.

Results are unaffected by small variations in stress (14 to 18 psi) and reinforcement ratio (0.007 to 0.009) if considered significant to the nearest whole microstrain. The regression model error is represented as E, with a standard error of +/- 0.8 με, and a model coefficient of determination equal to 0.13, which is reflective of the range of prediction data variability. The dashed lines in Fig. 5 represent the upper and lower bounds of a 95 % confidence interval, which were determined by computing regression model results for all 16,940 combinations of the independent variable ranges and adding the standard error multiplied by 1.96 (Mendenhall & Sincich [19]). The limits of these bounds span between about −4 με to 1 με, indicating regression model results fall roughly within this range when evaluated at the 95 % confidence level. Some model data points with lower values of t_r and t and higher values of m extend beyond these bounds, indicating regression model results may not completely capture some of these larger variations.

For comparison purposes, when inputting values from Table 5 to Eq. [6] shown in Fig. 5, a χ value equal to −0.7 με is computed. If evaluated at a 95 % confidence level and rounded to the nearest whole microstrain, a range between −2 με and + 1 με is found. The result of −1.14 με from Table 5 falls within this range. Because the time parameters in the model are specific to an individual segment, they need to be adjusted for the model to accommodate any segment within the tower. Each time parameter is adjusted by t_q, which represents the time the bottom story of segment q was poured:

$$\chi_q(t_r, t, m) = 1.8 + 0.01(t_r - t_q) - 0.4\ln(t - t_q) - 0.17(m) + E \quad [7]$$

5. Project measurements, results, and discussion

Salesforce Tower core walls were instrumented at nine separate levels (3, 5, 13, 21, 28, 36, 44, 48, and 55), totaling 36 gauges. Of these, only 16 gauges provided usable data throughout the project duration (Table 6). Lack of timely power sources led to a delay in Level 21 measurements and the inability to collect any measurements at levels 44, 48, and 55. One of the gauges reported inconsistent measurements,

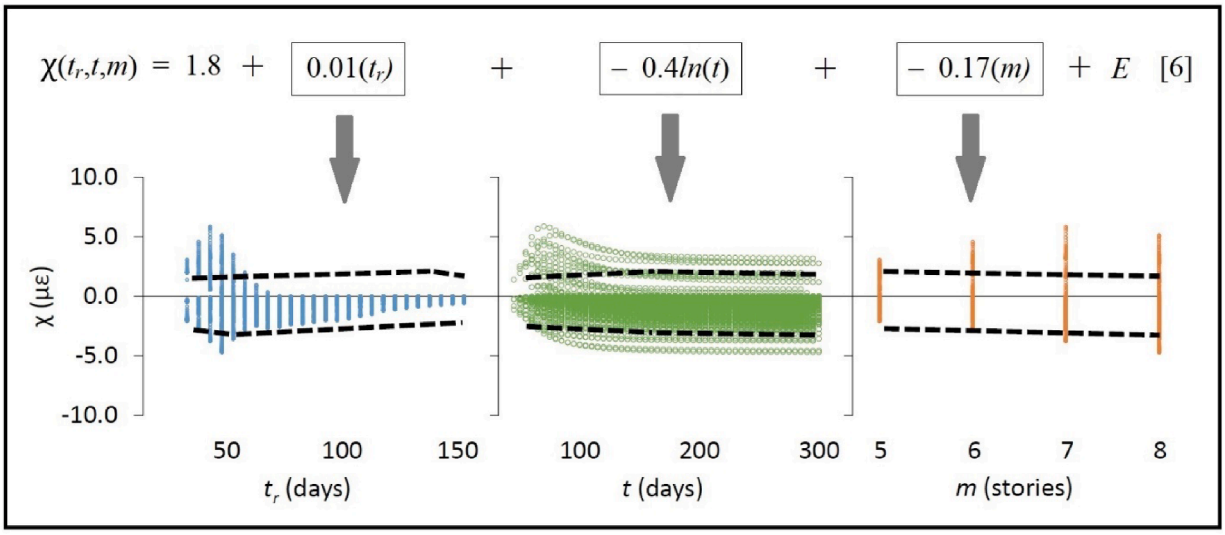

Fig. 5. Regression Model Data and 95% Confidence Interval Bounds.

Table 6
Measurement Acquisition.

Level	North Wall	South Wall	East Wall	West Wall
3	*[1]	✓	✓	✓
5	✓	✓	✓	✓
13	*[2]	✓	–[3]	✓
21	–[3]	–[3]	*[4,5]	*[4]
28	✓	✓	✓	✓
36	✓	–[3]	–[3]	✓
44	–[6]	–[6]	–[6]	–[6]
48	–[6]	–[6]	–[6]	–[6]
55	–[6]	–[6]	–[6]	–[6]

✓ Complete measurement dataset acquired.
* Partial measurement dataset acquired.
- No measurement dataset acquired.
[1] Sensor stopped reporting measurements on day 294 of the project timeline.
[2] Sensor measurements were inconsistent with others and stopped reporting measurements on project day 294.
[3] Sensor was likely damaged or malfunctioned and reported no measurement data.
[4] Delay in early sensor measurements due to lack of power supply.
[5] Sensor stopped reporting measurements on day 269 of the project timeline.
[6] No power supply was provided within sufficient timeframe to collect measurement data.

five others never reported any measurements, and two others stopped reporting measurements mid-project. Some of the gauge cabling potentially interfered with construction operations and was observed to have been physically cut, which likely accounts for the gauges that stopped working, whereas the gauges that never reported measurements were likely damaged during concrete placement. Some measurement gaps were also observed periodically at all levels, likely due to temporary power interruptions. In general, gauge measurements that were successfully acquired at each level varied by about ± 10 % of average. Measurements were averaged together, gaps in data were linearly interpolated, and averaged predictions were supplemented during the period of delay at Level 21.

Fig. 6A presents only prediction model results for Parking Level P3 because construction began before a gauge could be installed. This level is located three levels below grade, represents the tower's base, and was constructed on day zero of the project timeline (x-axis). Due to a lack of measurements at this level, average predicted values were used when calculating shortening estimations. CTE adjusted strain gauge measurements for Levels 3 and 5 are presented in Fig. 6B and 6C, respectively, and prediction model results were overlaid for comparison. In general, the measurements trended closely with the average of all prediction models results, providing some validation of an intrinsic link between measured and predicted strains. Other integration methods (e.g. Gausian or Newton-Cotes) might also be worthwhile to explore relative to improved predictions in future works.

5.1. Sample shortening estimations

Method C estimation results for the Level 5 elevation benchmark are presented in Table 7 and illustrated in Fig. 7. The benchmark elevation was established approximately 10 days after the story was poured, which coincides with day 117 of the project timeline. Shortening between t_r equal to 117 days and t equal to 347 days (when Level 61 was poured and monitoring concluded) is presented.

Segment 1 spans between Level P3 at the base of the tower and Level 3. Using values obtained from Fig. 6A and 6B, the measured change in strain occurring within Levels P3 and 3 were computed as 238 με and 294 με, respectively. The approximate non-linearity adjustment was computed using Eq. [7] as −0.2 ± 1.6 when evaluated at a 95 % confidence level. It should be noted that substantial delays were encountered during construction of Segment 1, resulting in story construction averaging approximately 17 days compared to 5 days assumed in the regression model. The approximate average change in strain was computed using Equation [2] as 265.8 ± 1.6 με, and shortening was estimated by multiplying the approximate average change in strain by the segment height per Equation [3] as 0.0255 ± 0.0002 ft (7.87 ± 0.06 mm).

Segment 2 spans between Level 3 and Level 5. Using Fig. 6C, the measured strain change occurring within Level 5 was computed as 309 με. The approximate non-linearity adjustment was computed using Equation [7] as 0.3 ± 1.6 when evaluated at a 95 % confidence level. It should be noted that an m equal to 2 stories falls below the 5-story parameter lower limit in the regression model. The approximate average change in strain was computed using Equation [2] as 301.8 ± 1.6 με and shortening was estimated by multiplying the approximate average change in strain by the segment height per Equation [3] as 0.0114 ± 0.0001 ft (3.47 ± 0.03 mm). Cumulative shortening of both segments was then computed using Equation [4] as 0.037 ft (11.3 mm) and the benchmark elevation at the top of Segment 2 at time t was accordingly updated using Equation [5] as 78.673 ft (23.980 m).

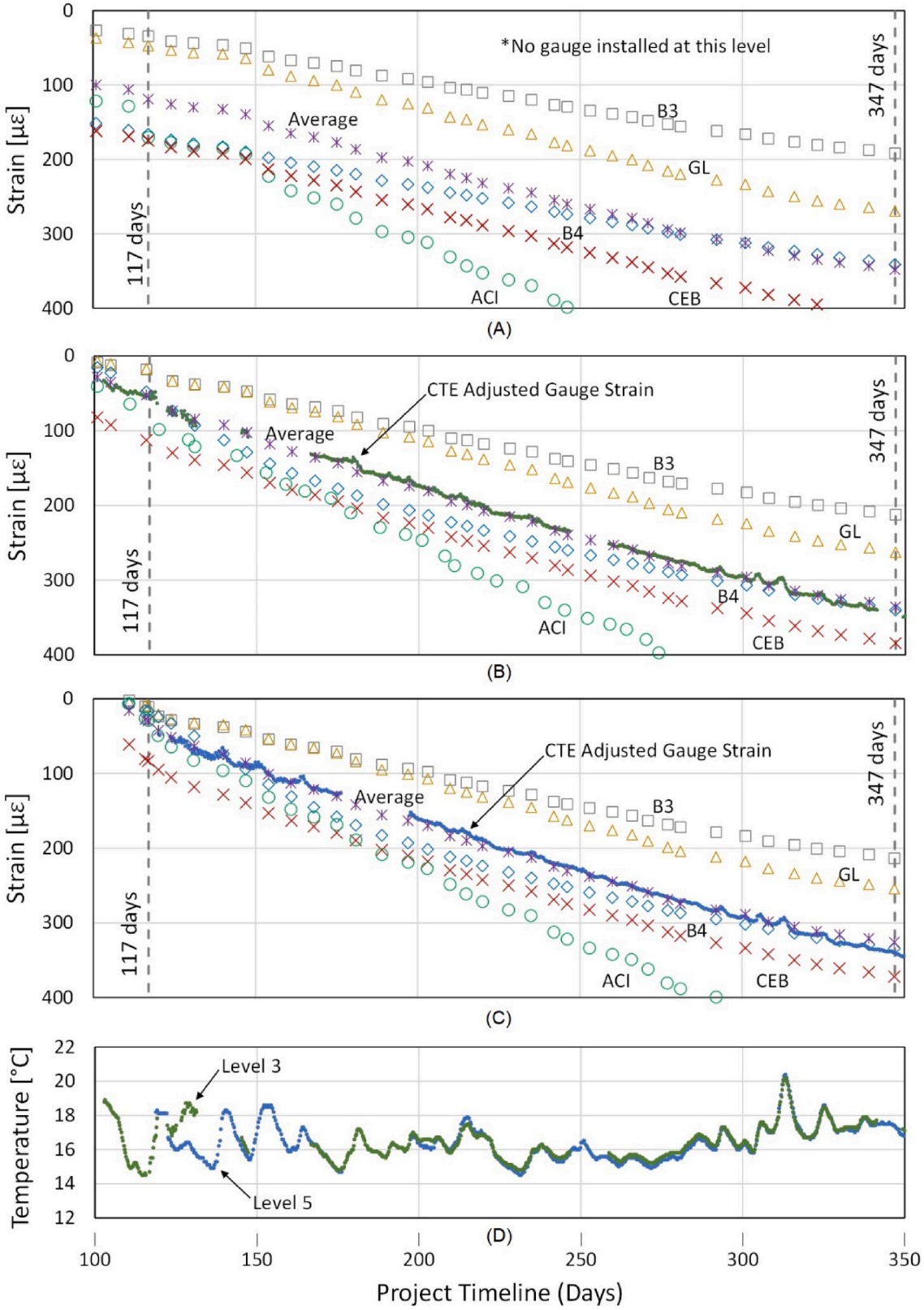

Fig. 6. (A) Level P3 Predicted Strain, (B) Level 3 Measured and Predicted Strain, (C) Level 5 Measured and Predicted Strain, (D) Measured Gauge Temperature.

5.2. Discussion of results

Fig. 8 illustrates cumulative shortening at benchmark levels (L3, L5, L13, L21, L28, L36) throughout construction based on Method C estimations. As expected, the trends indicate the rate of shortening increases with higher tower levels. Also overlaid on Fig. 8 are shortening values, specific to benchmarks at Levels 3 and 5, that were periodically gathered early in the project timeline using conventional total station instrumentation for purposes of validating strain-based results. The strain-based estimations agreed within the conventional measurement range

Table 7
Method C Estimations for Segments 1 and 2 (t_r = 117 days; t = 347 days).

	Segment 1 [q = 1]	Segment 2 [q = 2 = p]
$\varepsilon_1(t)$ [με]	358	348
$\varepsilon_1(t_r)$ [με]	120	54
$\varepsilon_m(t)$ [με]	348	339
$\varepsilon_m(t_r)$ [με]	54	30
$\Delta\varepsilon_1(t,t_r)$ [με]	238	294
$\Delta\varepsilon_m(t,t_r)$ [με]	294	309
$\chi_q(t_r,t,m)$ [με]	−0.2 ± 1.6	0.3 ± 1.6
$\overline{\Delta\varepsilon_q}(t,t_r)$ [με]	265.8 ± 1.6	301.8 ± 1.6
h_q [ft | m]	96.095 | 29.290	37.615 | 11.465
$\Delta h_q(t, t_r)$ [ft | mm]	0.0255 ± 0.0002 | 7.87 ± 0.06	0.0114 ± 0.0001 | 3.47 ± 0.03
$\Delta H_p(t, t_r)$ [ft | mm]	–	0.037 | 11.3
$EL_p(t_r)$ [ft | m]	–	78.710 | 23.991
$EL_p(t)$ [ft | m]	–	78.673 | 23.980

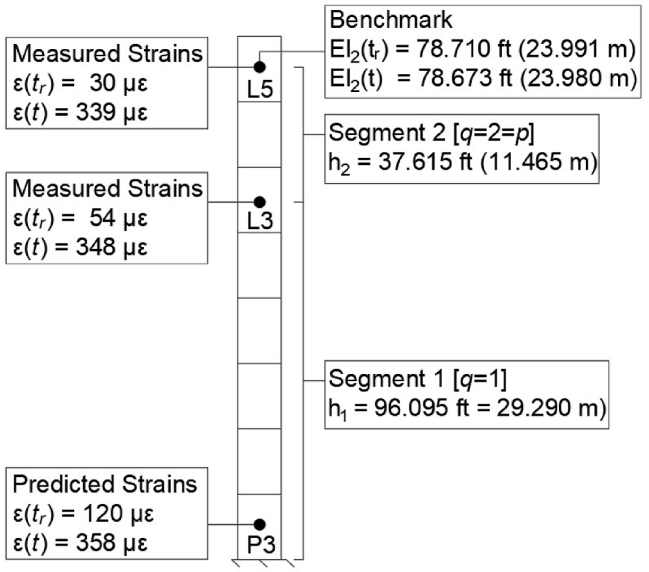

Fig. 7. Method C Estimations for Segments 1 and 2 (t_r = 117 days; t = 347 days).

of error, estimated to be on the order of +/-0.015 feet (+/-4.6 mm) by the project surveyor. For example, on day 347 of the project timeline, shortening at Level 5 was conventionally measured as −0.046 feet (-14.0 mm). After incorporating the estimated survey error, a range of values between −0.061 feet (-18.6 mm) and −0.031 feet (-9.4 mm) is computed. The strain-based shortening estimation equal to −0.037 feet (-11.3 mm) can be observed to fall within this range. Although the strain-based elevation monitoring method was used almost exclusively through Level 36, due to disruptions in the power systems previously discussed, additional conventional surveys were required at higher levels.

The strain-based elevation monitoring system up-front equipment and installation cost (on the order of $80,000) was offset by a significant reduction in survey labor (on the order of 400 h), resulting in an estimated net reduction in overall monitoring costs of at least 15 % (on the order of $25,000). More importantly, the efficiency gained through automation reduced the potential for survey related construction delays. It is estimated that taller towers will experience greater relative benefit, with cost reductions of at least 40 % (on the order of $150,000) for buildings roughly 100 stories tall.

Fig. 9A illustrates differences between Methods A and B shortening estimations at each benchmark level (L3, L5, L13, L21, L28, L36). The only difference between the two methods is the CTE adjustment in Method B. The most substantial variation to note is around day 312 when a spike in gauge temperature on the order of 6 °C occurred. Because Method A estimations do not adjust for temperature fluctuations, the readings registered an apparent strain reduction. The greatest impact was on Level 36 shortening, temporarily reflecting a reduction of approximately 0.0014 feet (0.43 mm). It is understandable that higher tower levels would experience greater effects since their shortening is an accumulation of all lower levels.

Fig. 9B illustrates differences between Methods B and C shortening estimations. The only difference between the two methods is the approximate non-linearity adjustment in Method C, which includes a range of error based on a 95 % confidence interval. The upper and lower bounds for each level in Fig. 9B illustrate this range of error. Ranges for higher tower levels are greater because they accumulate all error below them. The upper and lower bounds for each level are approximately centered around zero indicating the non-linearity adjustments themselves had only a minor effect on the shortening estimations, and that the key benefit of Method C is a better understanding of the level of

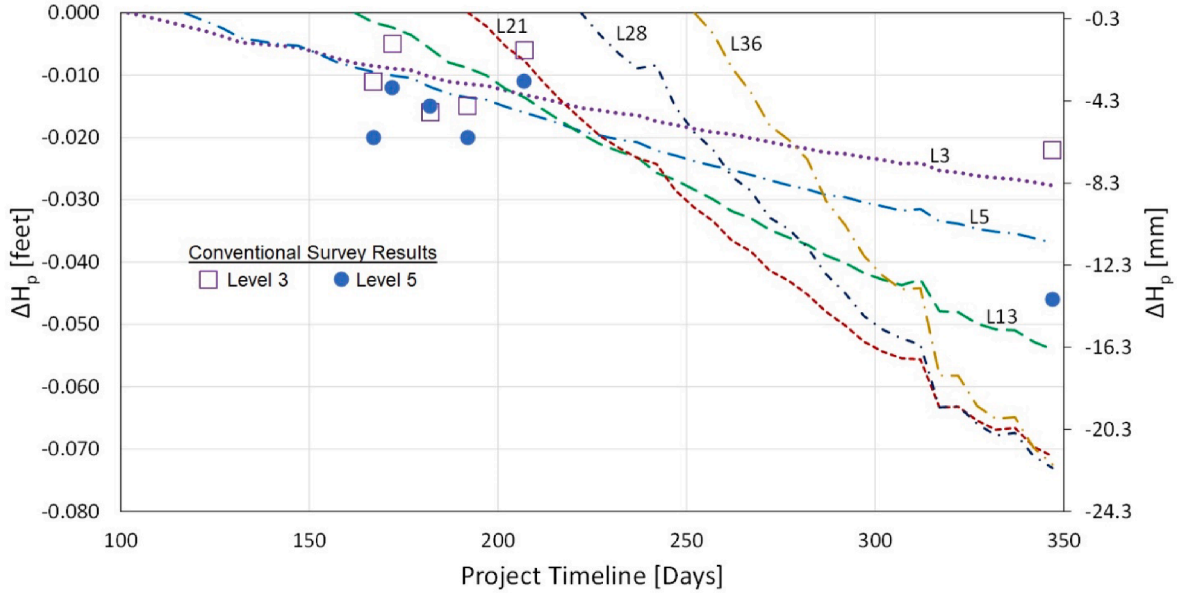

Fig. 8. Method C Shortening Estimations at Benchmark Levels.

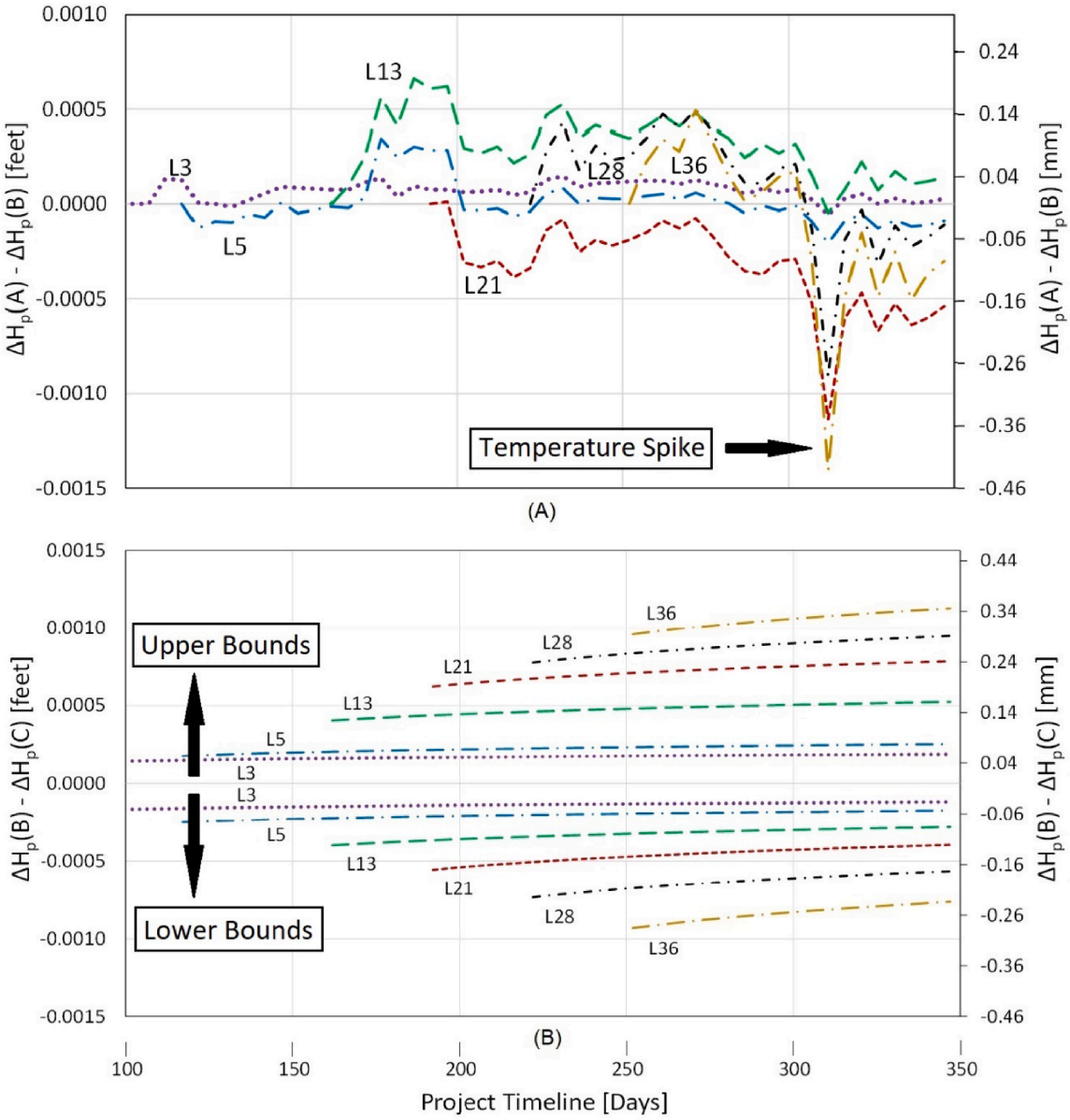

Fig. 9. (A) Difference between Methods A and B Estimations, and (B) Difference between Methods B and C Estimations.

uncertainty that exists in the estimates. Although the error range of about ± 0.001 ft (±0.30 mm) exhibited by Level 32 may be minor in survey terms, error ranges will continue to compound at higher tower levels, producing results of greater significance.

Additionally, error range significance becomes more apparent when comparing differences between Methods A and C, which can be computed by summing corresponding data from Fig. 9A and 9B ([A-B] + [B-C] = [A-C]). For example, the difference of −0.0014 feet (-0.43 mm) at Level 36 on day 312 from Fig. 9A summed with the −0.0008 feet (-0.24 mm) value from Fig. 9B for the lower range of Level 36 on the same day, gives a total difference of −0.0022 feet (-0.67 mm), indicating Method A shortening estimations errors can become large when temperature fluctuations occur, particularly at higher levels in the tower.

Lessons learned throughout the measurement acquisition process indicated the need for a more thoroughly coordinated sensor installation plan well before core wall construction is set to begin. Strain gauges should be protected from damage during concrete placement, which is very feasible and does not require investigation of alternative technologies. Power and data acquisition could benefit from improvements in either use of current methods (power sources and cabling) or implementation of emerging technologies (wireless and battery free sensing) discussed in the following paragraph. If traditional methods are used, power systems should be in place so there is no delay in initiating the data logging process after an instrumented story is cast and wiring should be laid out so that it does not interfere with other phases of construction.

A key factor for data acquisition being at a 44 % success rate was the lack of power supplies and cable damage during construction. As such, cable-free and battery-free sensing solutions emerge as promising alternatives (Chang & Hung [20]). In recent studies (Luo et al. [21], Gong et al. [22]), researchers introduced innovative techniques to wirelessly charge sensors that are embedded within concrete structures. When a reading from the sensor is required, a mobile reader is positioned close to the concrete wall. This allows the reader to charge the embedded sensor/monitoring system and wirelessly collect sensor readings. Furthermore, as reported by Lynch et al. [23], as much as 25 % of the total system expense was used for setting up a system to wire to an external power source, and more than 75 % of the installation time focused exclusively on the wiring procedure. The adoption of cable-free and battery-free sensors could significantly enhance the reliability and

viability of the strain-based elevation monitoring system (e.g., addressing the disruptions in the power systems) as well as structural health monitoring. A limitation of these systems is that they necessitate the use of low-power sensing solutions, but their potential should be investigated over time for monitoring programs like the one described herein.

6. Numerical analysis

The basis of the work presented thus far was not numerical modeling focused as a review of literature and a state-of-the-art assessment suggests physical measurements of shrinkage (i.e. shortening) of large structures is more lacking than numerical simulations. A second reason for less reliance on numerical modeling was this paper focused on developing shortening prediction methods that could be implemented during construction when time is of the essence. Significant advancements have been made in material models (e.g. Cai et al. [24]), and geometrical models (e.g. Chen et al. [25], Chen et al. [26]) over the past five years. Models of this level of sophistication, however, expend computational time and could impede effectiveness during construction. The work of this paper, on the other hand, could conceivably be integrated into a numerical routine that is made into a phone app (or equivalent). There are also studies showing how alternative surveying methods can be used effectively in conjunction with modeling. Micelli and Cascardi [27] used drone-based technology to perform surveys of a large masonry building where the results were input into a finite element code for structural modeling. The drone was used for a variety of reasons including safety and efficiency.

Several large and relevant numerical studies have been performed on concrete strain/shrinkage; some of the more recent and relevant examples are as follows. Faxiong et al. [28] used Abaqus to develop a creep and shrinkage analysis program roughly ten years ago. Even at this time, there were several numerical efforts cited regarding creep and shrinkage numerical modeling efforts. Testing of beams spanning 3 to 4 m with cross sectional dimensions of 100 to 200 mm per dimension were evaluated and the program was reported to be successful.

Bal and Buyle-Bodin [29] employed most of the strain/shrinkage prediction models of Table 2 to train/validate an Artificial Neural Network (ANN) in conjunction with shrinkage data extracted from the RILEM database. The study was reported to be successful. Zhu et al. [30] addressed creep and shrinkage by way of a convolutional neural network (CNN) that was verified by hundreds of sets of data in the Northwestern University database. CNN findings were used to develop an Abaqus user subroutine for simulating concrete creep and shrinkage that was validated by way of concrete beams with dimensions of 100 by 150 by 3750 mm.

Yeung et al. [31] investigated the applicability of the ACI 209 model for calcium sulfoaluminate cements in an experimental study and found that the model can be adopted by using different coefficients for different products than what were originally envisioned upon model development. Zhou et al. [32] studied high strength concrete (roughly 70 to 90 MPa at 28 day cure), which is representative of the compressive strengths in the Salesforce Tower walls. Multiple models from Table 2 were part of this evaluation. Physical shrinkage tests were performed on small specimens (515 by 100 by 100 mm). A theoretical model was developed based on linear superposition principles that was reported to successfully derive creep specific results with certain stress relaxation. This study showed that existing models typically overestimated specific creeps of the high-strength concretes.

In present day, commercially available software (e.g. Bentley RAM Connect) has implemented ACI 209's creep and shrinkage models for the purpose of slab design. Given the number of numerical modeling advancements made in this field, as presented in this section, this work aims to progress the acquisition of experimental data from actual large structures.

7. Summary, Conclusions, and Recommendations

This case study documented the successful implementation of a strain-based elevation monitoring system into reinforced concrete walls during construction of the 326 m tall Salesforce Tower in San Francisco, California. This system utilizes strain gages embedded into the tower's reinforced concrete walls at intermittent levels and the resulting measurements are inputs into one of three shortening estimation models (A to C) that were developed to balance the robustness needed from prediction models with the expediency needed during construction. Given the need for structural health monitoring, the successful outcomes documented in this paper, and the potential for continued improvement by way of, for example, wireless and battery free sensing technologies, the work documented herein is believed to be an incremental advancement to the state-of-the-art of tall buildings.

Conclusions from this work are:

1. The shortening estimation models were in agreement with conventional survey measurements (±4.6 mm) within their recommended tower height and temperature range capabilities and were a successful compliment to traditional surveying techniques.
2. Method A is the simplest approach, and is best suited for environments with mild temperature fluctuations (<10 °C).
3. Method B is of intermediate simplicity as it adjusts for temperature fluctuations and is adequate for moderately tall towers (<60 stories).
4. Method C is the most complex approach, adjusts for approximate non-linearity in concrete strain development between instrumented levels, provides a range of error in estimation results, and can be used for an array of conditions including towers taller than 60 stories.
5. Implementation of this system resulted in a net monitoring cost reduction on the order of 15 %, 400 labor hours reduced, and less potential for project delays.
6. Improvements are needed for supplying power to the sensors as there were interruptions, cut cables, and lack of power sources that led to a 44 % sensor success rate.

Recommendations for future work are:

1. Investigate the use of emerging cable and battery free sensor technologies as their use could improve effectiveness during construction, but could also allow the sensors installed to be used for structural health monitoring post construction.
2. Incorporate Methods A to C into future work in some manner where concrete cast with large volume to surface ratios is present. Additional data from projects like the Salesforce Tower only stands to strengthen the relationships between measured and predicted strains.

Declaration of Competing Interest

The authors declare that they have no known competing financial interests or personal relationships that could have appeared to influence the work reported in this paper.

Data availability

Data will be made available on request.

Acknowledgements

A special thanks to core wall project surveyor Kevin Stein and core wall construction manager Jim Klinger for supporting the design, installation, and validation of the strain-based system.

References

[1] Domosh M. The symbolism of the skyscraper: case studies of New York's first tall buildings. J Urban Hist 1988;14(3):320–45.

[2] Council on Tall Buildings and Urban Habitat [CTBUH] Skyscraper Center. (2022, July 25). *Skyscraper Database.* https://web.archive.org/web/20221025163759/https://www.skyscrapercenter.com/buildings.

[3] Fintel, M., Ghosh, S.K., & Iyengar, H. (1987). *Column shortening in tall structures - prediction and compensation.* Portland Cement Association, ISBN 0-89312-083-9.

[4] Ghilani CD. Elementary surveying: an introduction to geomatics 2018;Vol. 15: 347–8.

[5] Peronto J, Sinn R, Huizinga M. Vertical shortening considerations in the 1 km tall Jeddah Tower. International Journal of High-Rise Buildings 2017;6(1):21–31.

[6] Abdelrazaq A. Validating the structural behavior and response of Burj Khalifa: synopsis of the full scale structural health monitoring programs. International Journal of High-Rise Buildings 2012;1(1):37–51.

[7] Geymayer HG. Strain meters and stress meters for embedment in models of mass concrete structures. US Army Corps of Engineers; 1968. Technical Report No. 6–811.

[8] Bakoss SL, Burfitt AJ, Cridland L. Measurement of strains in concrete members with vibrating wire strain gauges. Australian Road Research 1977;7(3):20–6.

[9] Hameed A, Fernando GF, Hetherington JG, Brown RD, Leng J, Barnes RA. Investigation of strain transfer to a sensor protection system embedded in concrete using finite element analysis. Mater Struct 2002;35(9):557–63.

[10] Bazant ZP. Mathematical modeling of creep and shrinkage of concrete. John Wiley and Sons; 1988. p. 99–215. ISBN 0 471920576.

[11] Bazant ZP, Baweja S. Creep and shrinkage prediction model for analysis and design of concrete structures: model B3. ACI Special Publications 2000;194:1–84.

[12] Gardner NJ, Lockman MJ. Design provisions for drying shrinkage and creep of normal-strength concrete. ACI Mater J 2001;98(2):159–67.

[13] American Concrete Institute [ACI] Committee 209. (2008). Guide for modeling and calculating shrinkage and creep in hardened concrete (ACI 209.2 R-08). *American Concrete Institute*.

[14] Comité Euro-International du Béton [CEB] (1999). *Structural concrete – textbook on behaviour, design and performance. Updated Knowledge of the CEB/FIP Model Code 1990, 2,* 37-52, Fédération Internationale du Béton.

[15] Bazant ZP, Jirasek M, Hubler MH, Carol I. RILEM draft recommendation: TC-242-MDC multi-decade creep and shrinkage of concrete: material model and structural analysis. model B4 for creep, drying shrinkage and autogenous shrinkage of normal and high-strength concretes with multi-decade applicability. Mater Struct 2015;48 (4):753–70.

[16] Batten, M., Powrie, W., Boorman, R., & Leiper, Q. (1999). Use of vibrating wire strain gauges to measure loads in tubular steel props supporting deep retaining walls. *Proceedings of the Institution of Civil Engineers-Geotechnical Engineering, 137* (1), 3-13.

[17] Soil Instruments, Ltd. 2018. (2022, November 20). https://web.archive.org/web/2/http://www.itmsoilsupport.com/manuals/Man142_Vibrating_Wire_Embedment_Strain_Gauge.pdf.

[18] Gribniak V, Kaklauskas G, Kliukas R, Jakubovskis R. Shrinkage effect on short-term deformation behavior of reinforced concrete–when it should not be neglected. Mater Des 2013;51:1060–70.

[19] Mendenhall W, Sincich T. Regression analysis: a second course in statistics 2012; Vol. 7:166–82. ISBN 0-321-69169-5.

[20] Chang CY, Hung SS. Implementing RFIC and Sensor Technology to Measure Temperature and Humidity Inside Concrete Structures. Constr Build Mater 2012;26 (1):628–37.

[21] Luo, Y., Pu, L., Wang, J., and Howard, I.L. (2023). "Enhancing In-Situ Structural Health Monitoring through RF Energy-Powered Sensor Nodes and Mobile Platform," *arXiv:2308.10343 [eess.SY]*.

[22] Gong, Z., Han, L., An, Z., Yang, L., Ding, S. and Xiang, Y. (2022). " Empowering Smart Buildings With Self-sensing Concrete for Structural Health Monitoring," *Proceedings of the ACM SIGCOMM 2022 Conference*, August, pp. 560-575.

[23] Lynch, J.P., Law, K.H., Straser, E.G., Kiremidjian, A.S. and Kenny, T.W. (2000). "The Development of a Wireless Modular Health Monitoring System for Civil Structures." *In MCEER Mitigation of Earthquake Disaster by Advanced Technologies (MEDAT-2) Workshop*, November.

[24] Cai W, Dou L, Ju Y, Cao W, Yuan S, Si G. A Plastic Strain-Based Damage Model for Heterogeneous Coal Using Cohesion and Dilation Angle. Int J Rock Mech Min Sci 2018;110:151–60.

[25] Chen Y, Xu R, Lu C, Liu K, Feng J, Sareh P. Multi-stability of the Hexagonal Origami Hypar Based on Group Theory and Symmetry Breaking. Int J Mech Sci 2023;247: 108196.

[26] Chen Y, Lu C, Yan J, Feng J, Sareh P. Intelligent Computational Design of Scalene-faceted Flat-foldable Tessellations. J Comput Des Eng 2022;9:1765–74.

[27] Micelli F, Cascardi A. Structural Assessment and Seismic Analysis of a 14th Century Masonry Tower. Eng Fail Anal 2020;107:104198.

[28] Faxiong, L., Jia, G., Houqing, H., Qian, L. (2013). "Concrete Creep and Shrinkage Effect Analysis Program Development," *Applied Mechanics and Materials,* doi.org/10.4028/www.scientific.net/AMM.405-408.

[29] Bal L, Buyle-Bodin F. Artificial Neural Network for Predicting Drying Shrinkage of Concrete. Constr Build Mater 2013;38:248–54.

[30] Zhu J, Wang Y. Convolutional Neural Networks for Predicting Creep and Shrinkage. Constr Build Mater 2021;306:124868.

[31] Yeung JSK, Yam MCH, Wong YL. Model for Predicting Shrinkage of Concrete Using Calcium Sulfoaluminate Cement Blended with OPC, PFA, and GGBS. Journal of Building Engineering 2020;32:101671.

[32] Zhou Y, Chen W, Yan P. Measurement and Modeling of Creep Property of High-Strength Concrete Considering Stress Relaxation Effect. Journal of Building Engineering 2022;56:104726.